Inorg. Chem. **2005**, *44*, 5388–5396

Photoinduced One-Electron Reduction of Alkyl Halides by Dirhodium(II,II) Tetraformamidinates and a Related Complex with Visible Light

Daniel A. Lutterman,[‡] Natalya N. Degtyareva,[‡] Dean H. Johnston,[§] Judith C. Gallucci,[‡] Judith L. Eglin,[†] and Claudia Turro*[,‡]

Department of Chemistry, The Ohio State University, Columbus, Ohio 43210, and Department of Chemistry, Otterbein College, Westerville, Ohio 43081

Received November 17, 2004

Various substituted dirhodium tetraformamidinate complexes, Rh_2(R-form)$_4$ (R = *p*-CF_3, *p*-Cl, *p*-OCH_3, *m*-OCH_3; form = *N*,*N*′-diphenylformamidinate), and the new complex Rh_2(tpgu)$_4$ (tpgu = 1,2,3-triphenylguanidinate) have been investigated as potential agents for the photoremediation of saturated halogenated aliphatic compounds, RX (R = alkyl group). The synthesis and characterization of the complexes is reported, and the crystal structure of Rh_2(tpgu)$_4$ is presented. The lowest energy transition of the complexes is observed at ∼870 nm and the complexes react with alkyl chlorides and alkyl bromides under low energy irradiation ($\lambda_{irr} \geq 795$ nm), but not when kept in the dark. The metal-containing product of the photochemical reaction with RX (X = Cl, Br) is the corresponding mixed-valent Rh_2(II,III)X (X = Cl, Br) complex, and the crystal structure of Rh_2(*p*-OCH_3-form)$_4$Cl generated photochemically from the reaction of the corresponding Rh_2(II,II) complex in $CHCl_3$ is presented. In addition, the product resulting from the dimerization of the alkyl fragment, R_2, is also formed during the reaction of each dirhodium complex with RX. A comparison of the dependence of the relative reaction rates on the reduction potentials of the alkyl halides and their C–X bond dissociation energies are consistent with an outer-sphere mechanism. In addition, the relative reaction rates of the metal complexes with CCl_4 decrease with the oxidation potential of the dirhodium compounds. The mechanism of the observed reactivity is discussed and compared to related systems.

Introduction

The photoinduced reactivity of transition metal complexes has been widely explored for numerous potential applications. The conversion of solar energy has been an area of intense research for several decades with schemes that include photoexcited $[Ru(bpy)_3]^{2+}$ (bpy = 2,2′-bipyridine) and related Ru(II) complexes,[1−5] as well as other mononuclear complexes,[6,7] bimetallic systems,[8−11] transition metal clusters,[12] and solid-state materials.[13−15] The excited states of transition metal complexes are also able to photocleave DNA,[16−20] act

* To whom correspondence should be addressed. E-mail: turro@chemistry.ohio-state.edu.
† Current Address: P.O. Box 1663 MS G740, Los Alamos National Laboratory, Los Alamos, NM 87545.
‡ The Ohio State University.
§ Otterbein College.

(1) Hammarstroem, L. *Curr. Opin. Chem. Biol.* **2003**, *7*, 666.
(2) Sun, L.; Hammarstroem, L.; Akermark, B.; Styring, S. *Chem. Soc. Rev.* **2001**, *30*, 36.
(3) Islam, A.; Sugihara, H.; Arakawa, H. *J. Photochem. Photobiol., A* **2003**, *158*, 131.
(4) Brewer, K. J. *Comments Inorg. Chem.* **1999**, *21*, 201.
(5) Danielson, E.; Elliott, C. M.; Merkert, J. W.; Meyer, T. J. *J. Am. Chem. Soc.* **1987**, *109*, 2519.
(6) McGarrah, J. E.; Eisenberg, R. *Inorg. Chem.* **2003**, *42*, 4355.
(7) Pelizzetti, E.; Serpone, N. *Homogeneous and Heterogeneous Photocatalysis*; D. Reidel: Boston, 1986.
(8) Kleverlaan, C. J.; Indelli, M. T.; Bignozzi, C. A.; Pavanin, L.; Scandola, F.; Hasselman, G. M.; Meyer, G. J. *J. Am. Chem. Soc.* **2000**, *122*, 2840.
(9) James, C. A.; Morris, D. E.; Doorn, S. K.; Arrington, C. A.; Dunbar, K. R.; Finnis, G. M.; Pence, L. E.; Woodruff, W. H. *Inorg. Chim. Acta* **1996**, *242*, 91.
(10) Gray, T. G.; Veige, A. S.; Nocera, D. G. *J. Am. Chem. Soc.* **2004**, *126*, 9760.
(11) Heyduk, A. F.; Macintosh, A. M.; Nocera, D. G. *J. Am. Chem. Soc.* **1999**, *121*, 5023.
(12) Petersen, J. D.; Gahan, S. L.; Rasmussen, S. C.; Ronco, S. E. *Coord. Chem. Rev.* **1994**, *132*, 15.
(13) Loi, M. A.; Denk, P.; Hoppe, H.; Neugebauer, H.; Winder, C.; Meissner, D.; Brabec, C.; Sariciftci, N. S.; Gouloumis, A.; Vazquez, P.; Torres, T. *J. Mater. Chem.* **2003**, *13*, 700.
(14) Kroon, J. M.; O'Regan, B. C.; van Roosmalen, J. A. M.; Sinke, W. C. *Handbook of Photochemistry and Photobiology*; American Scientific Publishers: Stevenson Ranch, CA, 2003.
(15) Gregg, B. A. *J. Phys. Chem. B* **2003**, *107*, 4688.
(16) Fu, P. K.-L.; Bradley, P. M.; Turro, C. *Inorg. Chem.* **2001**, *40*, 2476.

10.1021/ic048377j CCC: $30.25
Published on Web 06/25/2005

as probes of DNA structure,[21,22] act as agents in photodynamic therapy,[23−27] and can also be used in long-range electron transfer.[28] In addition, the photochemistry of transition metal complexes toward alkyl and aryl halides has been investigated extensively in environmental photoremediation.[29−33]

One successful method for photoactivated remediation makes use of the Fenton reaction.[34−36] In the photo-Fenton system, acidic solutions of Fe(III) are photolyzed to generate Fe(II) and hydroxyl radicals.[34−36] With excess H_2O_2 present, the Fe(II) is reoxidized to Fe(III), thus making the process photocatalytic.[34−36] The photo-Fenton reaction has been found to successfully degrade pesticides, phenols, and halogenated hydrocarbons in water.[37−40] However, CCl_4 and other saturated perhalogenated aliphatic compounds do not react well with hydroxyl radicals.[41−44] Furthermore, these photoremediation processes require high-energy light in the UV or near-UV spectral region. Photochemistry initiated with visible and near-IR light is desirable for using the solar spectrum efficiently for such environmental transformations.

$Rh_2(O_2CCH_3)_4$ was recently shown to possess a long-lived excited state ($\tau = 4.6$ μs in CH_2Cl_2) that can be accessed with visible light ($\lambda_{exc} = 532$ nm).[45] An excited state oxidation potential, $E_{1/2}(Rh_2^{5+/4+*})$, of −0.5 V vs NHE is predicted for $Rh_2(OCCH_3)_4$ from $E_{1/2}(Rh_2^{5+/4+}) = +1.2$ V vs NHE in H_2O and $E_{00} \approx 1.7$ eV.[46] Although photoexcited $Rh_2(O_2CCH_3)_4$ is not expected to reduce alkyl halides in aqueous media, the related dirhodium(II) formamidinate complexes are easier to oxidize, with ground-state oxidation potentials that range from −0.094 to +0.424 V vs NHE.[47] Because of the shift in the oxidation potentials of these systems by 1.1−0.6 V relative to $Rh_2(O_2CCH_3)_4$, the excited states of the dirhodium formamidinate complexes are expected to be significantly better reducing agents, thus making it possible for these complexes to reduce alkyl halides upon irradiation with visible light. The photoreactivity of these complexes toward alkyl halides, if made catalytic, may be potentially useful for their decomposition.

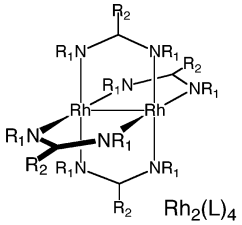

L	R_1	R_2
p-OCH_3-form	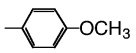	H
p-Cl-form	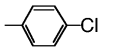	H
p-CF_3-form	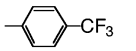	H
m-OCH_3-form	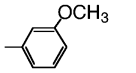	H
tpgu	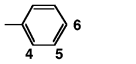	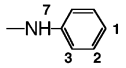

Figure 1. Molecular structures of $Rh_2(L)_4$ complexes.

The dirhodium tetraformamidinates, Rh_2(R-form)$_4$ (R = *p*-CF_3, *p*-Cl, *p*-OCH_3, *m*-OCH_3), whose structures are shown in Figure 1, absorb light throughout the visible region, with their lowest observable electronic transition at ∼870 nm. In addition, the variation of substituents on the formamidinate ligand provides a means to tune the oxidation potential of the complexes. The present work investigates the photoreactivity of the Rh_2(R-form)$_4$ (R = *p*-CF_3, *p*-Cl, *p*-OCH_3, *m*-OCH_3) series of complexes, as well as that of the related new complex $Rh_2(tpgu)_4$ (tpgu = 1,2,3-triphenylguanidinate), toward various alkyl halide substrates.

Experimental Section

Materials. $RhCl_3 \cdot xH_2O$ was purchased from Strem and used as received. Dichloromethane, chloroform, 1,2-dibromoethane, bromoform, carbon tetrabromide, carbon tetrachloride, dibromomethane, sodium acetate, *p*-chloroaniline, *p*-methoxyaniline, *p*-trifluromethylaniline, *m*-methoxyaniline, and triethylorthoformate were purchased from Aldrich and used without further purification. All other

(17) Fleisher, M. B.; Waterman, K. C.; Turro, N. J.; Barton, J. K. *Inorg. Chem.* **1986**, *25*, 3549.
(18) Pyle, A. M.; Long, E. C.; Barton, J. K. *J. Am. Chem. Soc.* **1989**, *111*, 4520.
(19) James, C. A.; Morris, D. E.; Doom, S. K.; Arrington, A.; Dunbar, K. R.; Finnis, G. M.; Pence, L. E.; Woodruff, W. H. *Inorg. Chim. Acta* **1996**, *242*, 91.
(20) Bradley, P. M.; Fu, P. K.-L.; Turro, C. *Comments Inorg. Chem.* **2001**, *22*, 393.
(21) Friedman, A. E.; Chambron, J. C.; Sauvage, J. P.; Turro, N. J.; Barton, J. K. *J. Am. Chem. Soc.* **1990**, *112*, 4960.
(22) Rehmann, J. P.; Barton, J. K. *Biochemistry* **1990**, *29*, 1701.
(23) Schaffer, M.; Schaffer, P. M.; Hofstetter, A.; Duehmke, E.; Jori, G. *Photochem. Photobiol. Sci.* **2002**, *1*, 438.
(24) Jones, B. U.; Helmy, M.; Brenner, M.; Serna, D. L.; Williams, J.; Chen, J. C.; Milliken, J. C. *Clin. Lung Cancer* **2001**, *3*, 37.
(25) Usuda, J.; Chiu, S.; Azizuddin, K.; Xue, L.-Y.; Lam, M.; Nieminen, A.-L.; Oleinick, N. L. *Photochem. Photobiol.* **2002**, *76*, 217.
(26) His, R. A.; Rosenthal, D. I.; Glatstein, E. *Drugs* **1999**, *57*, 725.
(27) Dougherty, T. J.; Gomer, C. J.; Henderson, B. W.; Jori, G.; Kessel, D.; Korbelik, M.; Moan, J.; Peng, Q. *J. Natl. Cancer Inst.* **1998**, *90*, 889.
(28) Supkowski, R. M.; Bolender, J. P.; Smith, W. D.; Reynolds, L. E. L.; Horrocks, W., Jr. *Coord. Chem. Rev.* **1999**, *185*−*186*, 307.
(29) Huston, P. L.; Pignatello, J. J. *Environ. Sci. Technol.* **1996**, *30*, 3457.
(30) Zepp, R. G.; Faust, B. C.; Hoigne, J. *Environ. Sci. Technol.* **1992**, *26*, 313.
(31) Haag, W. R.; Yao, C. C. D. *Environ. Sci. Technol.* **1992**, *26*, 1005.
(32) Watts, R. J.; Bottenberg, B. C.; Hess, T. F.; Jensen, M. D.; Teel, A. L. *Environ. Sci. Technol.* **1999**, *33*, 3432.
(33) Hislop, K. A.; Bolton, J. R. *Environ. Sci. Technol.* **1999**, *33*, 3119.
(34) Fenton, H. J. H. *Proc. Chem. Soc.* **1893**, *9*, 133.
(35) Fenton, J. H.; Jackson, H. J. *J. Chem. Soc.* **1899**, *75*, 1.
(36) Walling, C. *Acc. Chem. Res.* **1975**, *8*, 125.
(37) Lipczynska-Kochany, E. *Environ. Technol.* **1991**, *12*, 87.
(38) Pignatello, J. J. *Environ. Sci. Technol.* **1992**, *26*, 944.
(39) Sun, Y.; Pignatello, J. J. *Environ. Sci. Technol.* **1993**, *27*, 304.
(40) Rupert, G.; Bauer, R.; Heisler, G. *J. Photochem. Photobiol.* **1993**, *73*, 75.
(41) Legrini, O.; Oliveros, E.; Braun, A. M. *Chem. Rev.* **1993**, *93*, 671.
(42) von Sonntag, C.; Mark, G.; Mertens, R.; Schuchmann, M. N.; Schuchmann, H.-P. *Aqua* **1993**, *42*, 201.
(43) Buxton, G. V.; Greenstock, C. L.; Helman, W. P.; Ross, A. B. *J. Phys. Chem. Ref. Data* **1988**, *17*, 513.
(44) Guittonneau, S.; De Laat, J.; Dore, M.; Duguet, J. P.; Bonnel, C. *Rev. Sci. Eau* **1988**, *1*, 35.
(45) Bradley, P. M.; Bursten B. E.; Turro, C. *Inorg. Chem.* **2001**, *40*, 1376.
(46) Wilson, C. R.; Taube, H. *Inorg. Chem.* **1975**, *14*, 2276.
(47) Ren, T.; Lin, C.; Valente, E. J.; Zubkowski, J. D. *Inorg. Chim. Acta* **2000**, *297*, 283.

solvents were obtained from Fisher and used as received. Each formamidinate ligand was prepared by gently heating the corresponding aniline and triethylorthoformate, followed by washing with copious amounts of hexanes.[48] The ligand, 1,2,3-triphenylguanidine, was purchased from TCI America and was used as received. $Rh_2(\mu\text{-}O_2CCH_3)_4$, $Rh_2(p\text{-Cl-form})_4$, $Rh_2(p\text{-}OCH_3\text{-form})_4$, $Rh_2(p\text{-}CF_3\text{-form})_4$, and $Rh_2(m\text{-}OCH_3\text{-form})_4$ were prepared according to literature procedures.[47]

$Rh_2(tpgu)_4$. $Rh_2(O_2CCH_3)_4$ (0.6 mmol) and 1,2,3-triphenylguanidine (15 mmol) were added to a Schlenk vessel, placed under vacuum ($\sim 10^{-3}$ Torr), and heated at 160 °C for 8 h. The excess ligand was removed by washing the sample with copious amounts of acetone on a filter frit, and the product $Rh_2(tpgu)_4$ was dried under vacuum. The resulting olive green $Rh_2(tpgu)_4$ (tpgu = 1,2,3-triphenylguanidinate) solid was dissolved in dichloromethane and layered with methanol to produce dichroic green/purple crystals suitable for X-ray diffraction. MALDI-TOF/MS resulted in the parent ion peak at $m/z = 1350.3$ corresponding to $[Rh_2(tpgu)_4)]^+$. ^{1}H NMR (400 MHz) in THF-d_8 δ (splitting, integration, assignment from Figure 1): 6.20 (s, 4H, NH, **7**), 6.40 (d, 8H, central phenyl, **3**), 6.50 (t, 4H, central phenyl, **1**), 6.69 (t, 8H, central phenyl, **2**), 6.92 (t, 8H, phenyl, **6**), 6.97 (br, 16H, phenyl, **4**), 7.12 (t, 16H, phenyl, **5**). Anal. Calcd for $Rh_2N_{12}C_{76}H_{64}$: C, 67.55; N, 12.44; H, 4.77. Found: C, 66.94; N, 12.42; H, 4.86.

$Rh_2(p\text{-MeO-form})_4Cl$. $Rh_2(p\text{-MeO-form})_4$ was placed in a vial in $CHCl_3$ ($\sim$1 mM) and was allowed to slowly evaporate in room light. Over a 24 h period the green solution turned rusty brown and began to form X-ray quality crystals.

Instrumentation

Electronic absorption measurements were performed on a Hewlett-Packard diode array spectrophotometer (HP 8453) with HP 8453 Win System software. A 150 W Xe lamp (PTI LPS220) housed in a Milliarc compact arc lamp housing and powered by a Model LPS-220 lamp power supply was used in the steady-state photolysis experiments, and the wavelength of the light reaching the sample was controlled with 435, 515, and 715 nm long-pass filters (CVI). EPR spectra were collected on a Bruker spectrometer operating at 9.42 GHz at 120 K. The X-ray crystallography was performed on a Nonius Kappa CCD diffractometer at 200 K using an Oxford Cryosystems Cryostream Cooler.

^{1}H NMR spectra were recorded on Bruker NMR spectrometers (DPX-250 or DPX-400). Matrix-assisted laser desorption/ionization time-of-flight (MALDI-TOF) measurements were performed on a Bruker Reflex III mass spectrometer operated in the reflection positive ion mode with a N_2 laser. The electrochemistry measurements were performed on a Cypress Systems CS-1200 instrument with a single-compartment three-electrode cell. All samples were dissolved in dry dichloromethane at a concentration of approximately 10 mM with 0.1 M tetrabutylammonium hexafluorophosphate as the electrolyte. The working electrode was a 1.0 mm diameter Pt disk (Cypress or Bass) with a Pt-wire auxiliary electrode and a Ag/Ag^+ pseudo-reference electrode. All potentials were determined by reference to the ferrocene/ferrocenium couple.[49] The $E_{1/2}(Rh_2^{5+/4+})$ values were estimated using both cyclic voltammetry (scan rate = 100 mV/s) and differential pulse voltammetry (ΔE = 100 mV).

Methods. Photolysis experiments were conducted by adding the halogenated solvent to a given solid sample in the dark, followed by irradiation of the sample. Deoxygenation was performed either by bubbling the sample with argon for $\sim$15 min and keeping it under positive argon pressure during the experiment, or through three freeze−pump−thaw cycles. The reaction progress was monitored by changes in the electronic absorption spectrum as a function of irradiation time. The power dependence experiments were carried out using neutral density filters which absorbed 0.1, 0.5, 0.6, and 1.0 throughout the visible region.

Table 1. Crystallographic Data for $Rh_2(tpgu)_4$ and $Rh_2(p\text{-MeO})_4Cl$[a]

	$Rh_2(tpgu)_4$[b]	$Rh_2(p\text{-MeO})_4Cl$
chemical formula	$Rh_2C_{77}H_{66}C_{l2}N_{12}$	$Rh_2C_{60}H_{60}N_8O_8Cl$
fw (g mol^{-1})	1436.14	1262.43
space group	*C*2/*c*	*P*4/*ncc* (No. 130)
a (Å)	18.5107(3)	14.135(1)
b (Å)	21.7505(4)	14.135(1)
c (Å)	16.6588(3)	30.314(4)
θ (deg)	96.433(1)	
vol (Å^3)	6664.9(2)	6056.7(10)
Z	4	4
D_{calcd} (g cm^{-3})	1.431	1.384
μ (mm^{-1})	0.630	0.647
R (F_o)[c]	0.0369	0.0402
R_w (F_o^2)[d] (all data)	0.0935	0.1136

[a] Collected at 200(2) K with a wavelength of 0.71073 Å. [b] Complex + CH_2Cl_2. [c] $I > 2\theta(I)$, $R = \sum(|F_o| - |F_c|)/\sum|F_o|$. [d] $R_w = [\sum w(F_o^2 - F_c^2)^2/\sum w(F_o^2)^2]^{1/2}$, where $w = 1/[\sum^2(F_o^2) + (xP)^2 + yP]$, $P = (F_o^2 + 2F_c^2)/3$, $x = 0.0434$ and $y = 9.2457$ for $Rh_2(tpgu)_4 + CH_2Cl_2$, and $x = 0.0491$ and $y = 4.5459$ for $Rh_2(p\text{-MeO-form})_4Cl$.

Examination of the X-ray diffraction pattern indicated monoclinic and tetragonal crystal systems for $Rh_2(tpgu)_4$ and $Rh_2(p\text{-MeO-form})_4Cl$, respectively. The data collection strategy was designed to measure a quadrant of reciprocal space with a redundancy factor of 4.5 for $Rh_2(tpgu)_4$ and 3.3 for $Rh_2(p\text{-MeO-form})_4Cl$ so that 90% of the reflections in each quadrant were measured at least 4.5 or 3.3 times, respectively. A combination of φ and ω scans with a frame width of 1.0° was used. Data integration was performed with Denzo,[50] and scaling and merging of the data was performed with Scalepack.[50] Merging the data and averaging the symmetry equivalent reflections resulted in a R_{int} value of 0.056 for $Rh_2(tpgu)_4$ and 0.053 for $Rh_2(p\text{-MeO-form})_4Cl$. Cell parameters and refinement results for both complexes are summarized in Table 1.

$Rh_2(tpgu)_4$ was determined to be *C*2/*c* by the teXsan package[51] on the basis of systematic absences and the intensity statistics. The structure was solved by the Patterson method in SHELXS-86,[52] where the Rh atom was located. With $Z = 4$, the Rh dimer possesses a crystallographic 2-fold rotation axis. The remaining non-hydrogen atoms were located by standard Fourier methods. A CH_2Cl_2 solvent molecule is also present in the asymmetric unit, and it is disordered about the 2-fold axis. Bond length restraints were used in modeling this disorder. Full-matrix least-squares refinements based on F^2 were performed in SHELXL-93.[53] The hydrogen atoms bonded to the nitrogen atoms were located on the difference electron density maps and were added to the model and refined isotropically. The remaining hydrogen atoms were included in the model at calculated positions using a riding model with $U(H) = 1.2U_{eq}$(attached atom). The final refinement cycle was based on all 7629 intensities and 432 variables and resulted in agreement factors of $R(F) = 0.060$

(48) (a) Bradley, W.; Wright, I. *J. Chem. Soc.* **1956**, 640. (b) Eglin, J. L.; Smith, L. T.; Staples, R. J. *Inorg. Chim. Acta* **2003**, *351*, 217.
(49) Rieger, P. H. *Electrochemistry*, 2nd ed.; Chapman & Hall: New York, 1994.
(50) Otwinowski, Z.; Minor, W. In *Methods in Enzymology*; Carter,C. W., Jr., Sweet, R. M., Eds.; Macromolecular Crystallography, Part A, Vol. 276; Academic Press: New York, 1997; pp 307−326.
(51) *TEXSAN: Crystal Structure Analysis Package*, version 1.7−2.; Molecular Structure Corporation: The Woodlands, TX, 1995.
(52) Sheldrick, G. M. *Acta Crystallogr., Sect. A* **1990**, *46*, 467.
(53) Sheldrick, G. M. *SHELXL-93*; Universitat Göttingen: Göttingen, Germany, 1993.

and $R_w(F^2) = 0.094$. For the subset of data with $I > 2\sigma(I)$, the $R(F)$ value was 0.037 for 5775 reflections. The final difference electron density map contained maximum and minimum peak heights of 0.84 and −0.95 e/Å^3, respectively. Neutral atom scattering factors were used and included terms for anomalous dispersion.[54]

For Rh_2(*p*-MeO-form)$_4$Cl, the space group was determined to be *P*4/*ncc* by the teXsan package.[51] This is a uniquely determined space group in the Laue group 4/*mmm*. The structure was solved by Patterson method in SHELXS-97,[55] where the Rh atoms were located. With $Z = 4$, the Rh dimer contains a 4-fold axis of rotation. The remaining non-hydrogen atoms were located by standard Fourier methods. Full-matrix least-squares refinements based on F^2 were performed in SHELXL-97.[55] There is a disordered region of solvent on the 4-fold axis for which it was not possible to obtain a reasonable model. Instead, the SQUEEZE[56] program of PLATON[57] was used to modify the observed structure factors by subtracting the contributions from the electron density in the disordered area. In this case, this disordered region occupied a total of 781 Å^3 per unit cell and amounts to 95 electrons/unit cell. The methyl group hydrogen atoms were added at calculated positions using a riding model with $U(H) = 1.5U_{eq}$(bonded C atom). For each methyl group, the torsion angle which defines its orientation about the O−C bond was refined. The remaining hydrogen atoms were included in the model at calculated positions using a riding model with $U(H) = 1.2U_{eq}$(attached atom). The final refinement cycle was based on all 3476 intensities and 183 variables and resulted in agreement factors of $R(F) = 0.071$ and $R_w(F^2) = 0.114$. For the subset of data with $I > 2\sigma(I)$, the $R(F)$ value was 0.040 for 2282 reflections. The final difference electron density map contained maximum and minimum peak heights of 0.83 and −0.73 e/Å^3, respectively. Neutral atom scattering factors were used and included terms for anomalous dispersion.[54]

The molecular and electronic structure determinations on the model complex $Rh_2(HNC(H)NH_2)_4$ were performed with density functional theory (DFT) using the Gaussian 98 program.[58] The B3LYP[59−61] functional along with the 6-31G* basis set for H, C, and N,[62] and the SDD energy-consistent pseudopotentials for Rh were used.[63] All geometries were fully optimized using the criteria of the respective programs. Orbital analyses were completed with GaussView.[64] Electronic transitions were calculated using the TDDFT methods implemented within Gaussian 98.

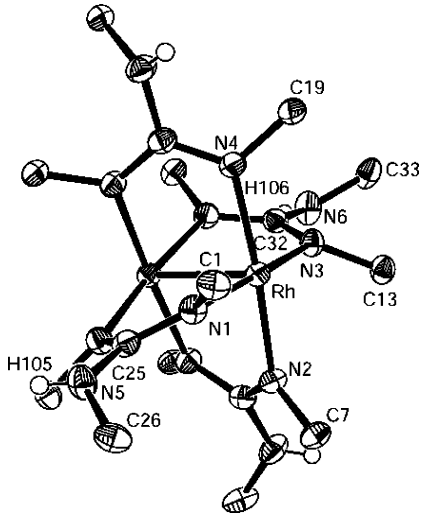

Figure 2. ORTEP representation of $Rh_2(tpgu)_4$ with thermal ellipsoids drawn at the 50% probability level. Only the core atoms of the complex and the ipso carbons of the phenyl rings are shown for clarity.

Results and Discussion

Synthesis and Characterization of $Rh_2(tpgu)_4$. $Rh_2(tpgu)_4$ was prepared from $Rh_2(O_2CCH_3)_4$ and 1,2,3-triphenylguanidine following a procedure analogous to that previously reported for the related dirhodium formamidinate complexes.[47] The characterization of the product was achieved through ^{1}H NMR in solution, mass spectrometry, and crystallography. The crystal structure of $Rh_2(tpgu)_4$ is shown in Figure 2. The Rh−Rh and Rh−N bond lengths are comparable to those of other dirhodium compounds with similar paddle wheel structures, including dirhodium formamidinates, which are listed in Table 2.[47,65−68]

The position and integration of the peaks in the ^{1}H NMR (400 MHz) spectrum of $Rh_2(tpgu)_4$ in THF-d_8 (Figure 3) were used to assign the resonances to the aromatic protons of the three phenyl rings and the NH of each ligand (numbering scheme from Figure 1). $Rh_2(tpgu)_4$ possesses phenyl rings similar to those of the dirhodium tetraformamidinate complexes, which aided in their assignment.[47] One key difference between the ^{1}H NMR spectrum of $Rh_2(tpgu)_4$ and other dirhodium(II) tetraformamidinate complexes is the presence of a resonance at 6.20 ppm assigned to the NH proton of the tpgu ligand. In $Rh_2(tpgu)_4$, the central $-N(H)C_6H_5$ group of the guanidinate ligand is significantly bulkier than the hydrogen atom found in the same position in the forma-

(54) Wilson, A. J. C.; Prince, E. *International Tables for Crystallography Volume C*; Kluwer Academic Publishers: Dordrecht, The Netherlands, 1992.
(55) Sheldrick, G. M. *SHELXL-97*; Universitat Göttingen: Göttingen, Germany, 1997.
(56) van der Sluis, P.; Spek, A. L. *Acta Crystallogr., Sect. A* **1990**, *46*, 194−201.
(57) Spek, A. L. *PLATON*; Utrecht University: Utrecht, The Netherlands, 2001.
(58) Frisch, M. J. S.; Trucks, G. W.; Schlegel, H. B.; Scuseria, G. E.; Robb, M. A.; Cheeseman, J. R.; Zakrzewski, V. G.; Montgomery, J. A., Jr.; Stratmann, R. E.; Burant, J. C.; Dapprich, S.; Millam, J. M.; Daniels, A. D.; Kudin, K. N.; Strain, M. C.; Farkas, O.; Tomasi, J.; Barone, V.; Cossi, M.; Cammi, R.; Mennucci, B.; Pomelli, C.; Adamo, C.; Clifford, S.; Ochterski, J.; Peterson, G. A.; Ayala, P. Y.; Cui, Q.; Morokuma, K.; Malick, D. K.; Rabuck, A. D.; Raghavachari, K.; Foresman, J. B.; Cioslowski, J.; Ortiz, J. V.; Stefanov, B. B.; Liu, G.; Liashenko, A.; Piskorz, P.; Komaromi, I.; Gomperts, R.; Martin, R. L.; Fox, D. J.; Keith, T.; Al-Laham, M. A.; Peng, C. Y.; Nanyakkara, A.; Gonzalez, C.; Challacombe, M.; Gill, P. M. W.; Johnson, B. G.; Chen, W.; Wong, M. W.; Andres, J. L.; Head-Gordon, M.; Replogle, E. S.; Pople, J. A. *Gassian 98*, revision A9; Gaussian, Inc.; Pittsburgh, PA, 1998.
(59) Becke, A. D. *Phys. Rev. A: Gen. Phys.* **1988**, *38*, 3098.
(60) Becke, A. D. *J. Chem. Phys.* **1993**, *98*, 5648.
(61) Lee, C.; Yang, W.; Parr, R. G. *Phys. Rev. B: Condens. Matter Mater. Phys.* **1988**, *37*, 785.
(62) Hehre, W. J.; Radom, L.; Schleyer, P. V. R.; Pople, J. A. *Ab initio Molecular Orbital Theory*; John Wiley & Sons: New York, 1986.
(63) Andrae, D.; Haeussermann, U.; Dolg, M.; Stoll, H.; Preuss, H. *Theor. Chim. Acta* **1990**, *77*, 123.
(64) Gaussian Inc.: Pittsburgh, PA, 1998.
(65) Bear, J. L.; Yao, C. L.; Lifsey, J. D.; Korp, J. D.; Kadish, K. M. *Inorg. Chem.* **1991**, *30*, 336.
(66) Bear, J. L.; Yao, C. L.; Liu, L. M.; Capdevielle, F. J.; Korp, J. D.; Albright, T. A.; Kung, S. K.; Kadish, K. M. *Inorg. Chem.* **1989**, *28*, 1254.
(67) He, L. P.; Yao, C. L.; Naris, M.; Lee, J. C.; Korp, J. D.; Bear, J. L. *Inorg. Chem.* **1992**, *31*, 620.
(68) Le, J. C.; Chavan, M. Y.; Chau, L. K.; Bear, J. L.; Kadish, K. M. *J. Am. Chem. Soc.* **1985**, *107*, 7195.

Table 2. Selected Bond Lengths of $Rh_2(tpgu)_4$ and $Rh_2(p\text{-MeO-form})_4Cl$ and Related Dirhodium Compounds

Compounds	Distance (Å)		
	Rh−Rh	Rh−N	Rh−Cl
$Rh_2(tpgu)_4$	2.4077(4)	2.056(2)	
$Rh_2(dpf)_4$[a]	2.459(3)	2.048(4)	
$Rh_2(dpba)_4$[b]	2.389(15)	2.050(2)	
$Rh_2(m\text{-MeO-form})_4$[c]	2.452(1)	2.415(1)	
	2.041(5)	2.055(5)	
$Rh_2(3,5\text{-}Cl_2\text{-form})_4$[c]	2.458(1)	2.05(1)	
$(4,0)Rh_2(ap)_4$[d]	2.412 (1)	2.04(3)[e]	
		2.03(2)[f]	
$Rh_2(p\text{-MeO-form})_4Cl$	2.4670(7)	2.046(2)	2.400(2)
$(4,0)Rh_2(ap)_4Cl$[d]	2.406(1)	2.008(1)[e]	2.421(3)
		2.048(3)[f]	
$(4,0)Rh_2(2\text{-F-ap})_4Cl$[g]	2.412(6)	2.007(3)[e]	2.431(1)
		2.063(3)[f]	
$(4,0)Rh_2(2,6\text{-}F_2\text{-ap})_4Cl$[g]	2.4157(9)	2.021(11)[e]	2.465(2)
		2.058(4)[f]	
$(3,1)Rh_2(2,6\text{-}F_2\text{-ap})_4Cl$[g]	2.4197(4)	2.021(3)[e]	2.444(1)
		2.055(3)[f]	
$(3,1)Rh_2(F_5\text{-ap})_4Cl$[g]	2.4153(6)	2.02(2)[e]	2.438(1)
		2.055(1)[f]	

[a] Ref 65; dpf = *N*,*N*′-diphenylformamidinate. [b] Ref 67; dpba = *N*,*N*′-diphenylbenzamidinate. [c] Ref 47; two molecules per asymmetric unit each with a different Rh−Rh and Rh−N distances. [d] Ref 66; ap = 2-anilinopyridine; (4,0) and (3,1) refers to the isomeric arrangement of the unsymmetrical ap ligand about the dirhodium core. [e] Anilino N. [f] Pyridyl N. [g] Ref 73.

midinate ligands. The broadening of the signal corresponding to the H4 protons (Figure 1) at 6.97 ppm can be attributed to the presence of a rotational barrier about the central C−N bond, resulting in various solution conformations that place the H4 proton at different positions in relation to the nearby NH (H7) proton. The increased mobility about the central C−N bond as the temperature is increased from 27 to 60 °C results in the sharpening and upfield shift of the H4 proton signal, with a concomitant upfield shift of the peak assigned to the NH proton (Figure 3). These results are consistent with a rotational barrier about the central C−N bond, likely caused by the steric bulk of the central phenyl group of the guanidinate ligand, which is not observed in the dirhodium formamidinate complexes.

Electronic Absorption and Ground-State Oxidation. The electronic absorption spectra of $Rh_2(R\text{-form})_4$ (R = *p*-CF_3, *p*-Cl, *p*-OCH_3, *m*-OCH_3) measured by us are consistent with those previously reported. The absorption maxima for these complexes and $Rh_2(tpgu)_4$ are listed in Table 3.[47] The lowest energy transition is observed at ~870 nm ($\epsilon \approx 1500\ M^{-1}\ cm^{-1}$), which was previously assigned in the dirhodium tetraformamidinate complexes to the $Rh_2(\pi^*) \rightarrow Rh_2(\sigma^*)$ transition.[69,70] Similar spectral features are observed for the new complex, $Rh_2(tpgu)_4$, with its lowest-energy transition at 878 nm ($\epsilon = 2990\ M^{-1}\ cm^{-1}$) in CH_2Cl_2. Time-dependent density functional theory (TDDFT) calculations on the model complex $Rh_2(HNC(H)NH)_4$ predict that the $Rh_2(\pi^*) \rightarrow Rh_2(\sigma^*)$ transition occurs at 986 nm, which is the lowest-energy transition with significant oscillator strength.

The $E_{1/2}(Rh^{5+/4+})$ values for the formamidinate complexes measured here are similar to those previously reported for each complex and are listed in Table 3.[47] Interestingly, the oxidation potential of $Rh_2(tpgu)_4$, $E_{1/2}(Rh_2^{5+/4+}) = -0.012$ V vs NHE, lies between those of $Rh_2(p\text{-MeO-form})_4$ and $Rh_2(m\text{-MeO-form})_4$. Because the guanidinate ligands are more electron rich than the formamidinate ligands, they make the dirhodium core easier to oxidize, thus resulting in oxidation potentials similar to those of the dirhodium complexes with formamidinate ligands with electron-donating substituents.

Comparison of the absorption maxima and oxidation potential of $Rh_2(tpgu)_4$ to those of the dirhodium(II,II) formamidinates show that the electronic structure of the coordinated guanidinate ligand is similar to that of the formamidinates. Other dirhodium paddle wheel compounds have also been reported with similar absorption spectra and oxidation potentials.[68]

Steady-State Photochemistry with Alkyl Halides. Marked changes in the electronic absorption spectra of $Rh_2(R\text{-form})_4$ (R = *p*-CF_3, *p*-Cl, *p*-OCH_3, *m*-OCH_3) and $Rh_2(tpgu)_4$ were observed upon photolysis with visible light in the presence of various alkyl chlorides and alkyl bromides as solvents. Typical photolysis experiments as a function of irradiation time ($\lambda_{irr} \geq 435$ nm) are shown in Figure 4 for $Rh_2(tpgu)_4$ in CCl_4 and CH_2BrCH_2Br. No spectral changes were evident in the dark at room temperature under conditions similar to those employed in the photochemical reactions or when the complexes were irradiated in nonhalogenated solvents, such as toluene.

Figure 4a shows the growth of absorption peaks at 450, 540, ~650 (shoulder), and 1090 nm as the photolysis of $Rh_2(tpgu)_4$ progresses in CCl_4 ($\lambda_{irr} \geq 435$ nm) with the concomitant decrease in intensity of the absorption of the starting material at 878 nm. The spectral changes shown in Figure 4a result in five isosbestic points at 410, 460, 470, 825, and 900 nm. The observed spectral changes of each complex in all chlorinated solvents are similar in peak position and intensity, and the maxima for the products obtained from the photolysis of each complex in CCl_4 are listed Table 3, along with the photochemical quantum yields, Φ, for the complexes in CCl_4. From the similarity in the spectral changes that result from the reaction of each complex with all chlorinated substrates, it may be concluded that the same type of metal-containing products that absorb in the 400−1100 nm range are formed in these reactions.

The photolysis of $Rh_2(tpgu)_4$ in CH_2BrCH_2Br ($\lambda_{irr} \geq 435$ nm) is shown in Figure 4b as a function of irradiation time. New absorption peaks appeared at 440, 560, 790, and 1090 nm as the photolysis progressed. The concomitant decrease in intensity of the absorption at 878 nm corresponding to the initial $Rh_2(tpgu)_4$ complex resulted in three isosbestic points at 390, 840, and 900 nm (Figure 4b). Similarly, when $Rh_2(p\text{-MeO-form})_4$ and $Rh_2(p\text{-}CF_3\text{-form})_4$ were irradiated in different brominated solvents, new absorption peaks appear in the visible and near-IR region. As is the case with the chlorinated halides, the photolysis of each complex with alkyl bromides results in similar spectral features corresponding to the same type of product.

(69) Cotton, F. A.; Feng, X. *Inorg. Chem.* **1989**, *28*, 1180.
(70) Piraino, P.; Bruno, G.; Schiavo, S. L.; Laschi, F.; Zanello, P. *Inorg. Chem.* **1987**, *26*, 2205.

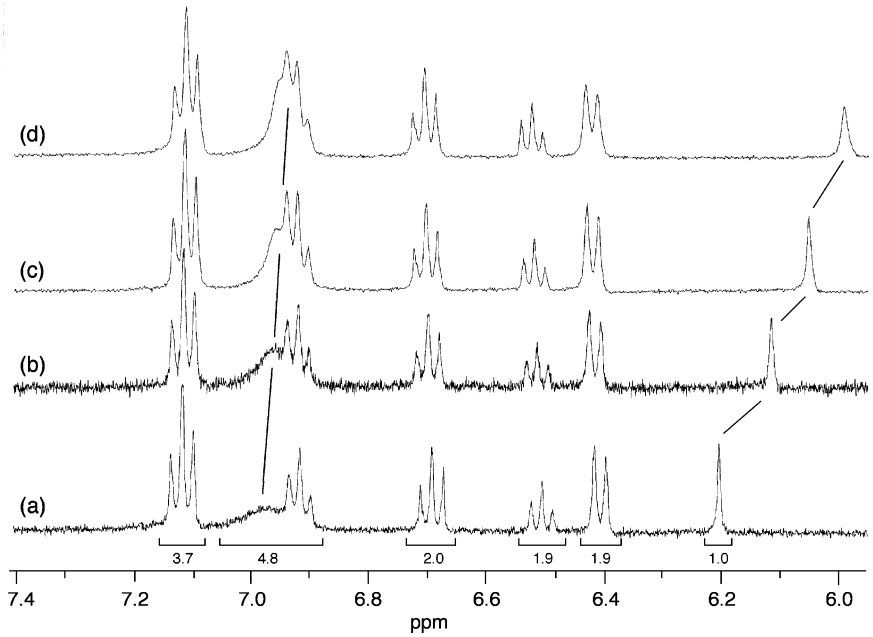

Figure 3. ^{1}H NMR of $Rh_2(tpgu)_4$ at (a) 25 °C with corresponding integrations, (b) 40 °C, (c) 50 °C, and (d) 60 °C in THF-d_8.

Table 3. Absorption (λ_{abs}) Maxima of Neutral $Rh_2(L)_4$ and One-Electron Oxidized Products from the Photolysis in CCl_4, $[Rh_2(L)_4]Cl$, Ground State Oxidation Potentials, and Photochemical Quantum Yields with CCl_4

	λ_{abs}/nm ($\epsilon \times 10^3$ M^{-1} cm^{-1})			
L	$Rh_2(L)_4$	$[Rh_2(L)_4]Cl$[b]	$E_{1/2}$/V[c]	Φ[d]
p-MeO-form	469(4.07), 586(0.80), 870(1.74)[a]	553(3.83), 996(4.34)	−0.094	*e*
m-MeO-form	473(3.75), 566(0.48), 867(1.52)[a]	562(2.36), 923(3.80)	−0.009	0.58
p-Cl-form	473(3.80), 576(0.77), 868(1.65)[a]	563(3.58), 949(4.84)	+0.194	0.32
p-CF_3-form	474(2.83), 564(0.66), 862(1.48)[a]	575(2.13), 945(2.72)	+0.424	0.044
tpgu	458(3.82), 600(0.35), 878(2.99)	542(3.88), 109(3.35)	−0.012	0.18

[a] Ref 47. [b] Generated from the photolysis of each complex in CCl_4 ($\lambda_{irr} = 435$ nm); ϵ values estimated from known concentration of reactant and following oxidation with $AgBF_4$. [c] $E_{1/2}(Rh_2^{5+/4+})$ in CH_2Cl_2 with 0.1 M tetrabutylammonium hexafluorophosphate vs NHE. [d] Photochemical quantum yield ($\lambda_{irr} = 450$ nm) using ferrioxalate as a standard (Murov, S. L; Carmichael, I.; Hug, G. L. *Handbook of Photochemistry, Second Edition Revised and Expanded*; Marcel Dekker: New York, 1993). [e] The presence of some thermal reactivity precludes the accurate measurement of the photochemical quantum yield.

It should be pointed out that irradiation with $\lambda_{irr} \geq 715$ nm resulted in identical photochemistry as that produced with higher-energy photons. For $Rh_2(tpgu)_4$, the reaction was 7 times slower with $\lambda_{irr} \geq 715$ nm than that it was under similar experimental conditions with $\lambda_{irr} \geq 495$ nm. When the area under the absorption curve was integrated in the 435−1100 nm and 715−1100 nm spectral regions, the area of the former was approximately 6.2 times greater than the latter. This result is consistent with a smaller number of photons being absorbed with lower-energy irradiation, resulting in a slower conversion to product.

The presence of several isosbestic points in the reaction of each dirhodium complex in the alkyl halide solutions is indicative of the formation of a single metal-containing product upon irradiation, without subsequent dark reaction or further photochemistry of the products. The power dependence of the reaction is consistent with a one-photon process where plots of log(*I*) vs log(rate) resulted in slopes of ∼1. Bubbling with argon for 30 min prior to photolysis and maintaining a positive argon pressure during the reaction do not affect the rate of conversion, indicating that oxygen is not involved in the mechanism. The dependence of the rates of the reactions on the concentration of dirhodium(II,-II) complex and alkyl halide indicate that the reactions are first order in each reactant.

Identification of the Product. The absorption maxima of the product obtained in the photochemical reaction of each complex in CCl_4 are listed in Table 3. The new absorption peak in each bimetallic product in the 900−1100 nm range is indicative of a one-electron oxidized Rh^{5+} dirhodium core.[70] An absorption maximum at 977 nm was previously reported for the mixed-valent $[Rh_2(2,6\text{-difluoroanilino})_4]^+$ cation.[71] Furthermore, the chemical oxidation of the dirhodium(II,II) tetraformamidinate complexes and $Rh_2(tpgu)_4$ with $AgBF_4$ result in cationic species with the characteristic near-IR absorption in the 900−1100 nm spectral region with maxima consistent with those observed in the products of the respective photochemical reaction (Table 3). For example, the electronic absorption spectrum of $[Rh_2(p\text{-}CF_3\text{-form})_4]^+$ prepared by stirring the corresponding Rh_2^{4+} complex with $AgBF_4$ in acetone for 1 h is compared to the photochemically generated product in CCl_4 in Figure 5a. The two spectra are nearly superimposable in

(71) Kadish, K. M.; Phan, T. D.; Girbabu, L.; Caemelbecke, E. V.; Bear, J. L. *Inorg. Chem.* **2003**, *42*, 8663.

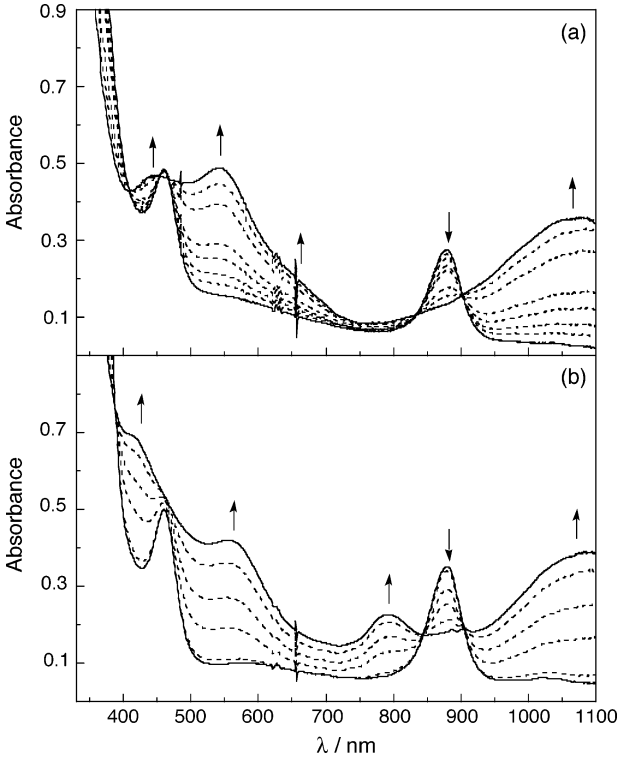

Figure 4. Changes to the electronic absorption spectra of $Rh_2(tpgu)_4$ upon irradiation (λ_{irr} = 435 nm) in (a) CCl_4 (0−120 min) and (b) CH_3CHBr_2 (0−1380 min).

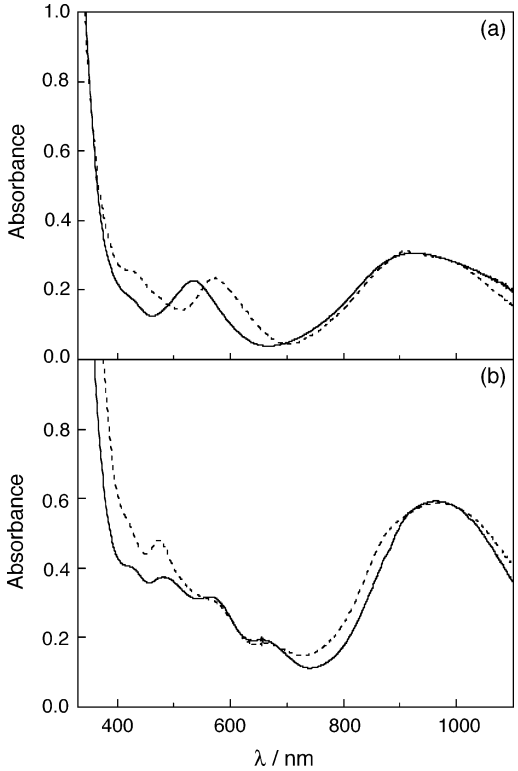

Figure 5. Electronic absorption spectra of (a) $Rh_2(p\text{-}CF_3\text{-form})_4$ oxidized photochemically (λ_{irr} = 435 nm, 5 min) in neat CCl_4 (dashed line) and with $AgBF_4$ in acetone (solid line) and (b) $Rh_2(m\text{-}OCH_3\text{-form})_4$ oxidized photochemically ($\lambda_{irr} \geq$ 435 nm, 5 min) with CBr_4 (30 mM) in acetone (dashed line) and with $AgBF_4$ in acetone (solid line) in the presence of $(t\text{-Bu})_4NBr$.

the 700−1100 nm region, however, a shift occurs in the peak from 535 nm in the chemically oxidized product to 570 nm in the photochemical reaction. As will be discussed in more detail below, this shift is likely to be the result of the coordination of a chloride ion in the axial position of the latter, whereas no axial coordination is expected in the former. Furthermore, the EPR spectrum recorded in dioxane at 77 K of the product resulting from the photochemistry of $Rh_2(p\text{-}CF_3\text{-form})_4$ in CCl_4 is consistent with that of the chemically generated $[Rh_2(p\text{-}CF_3\text{-form})_4]^+$ cation collected under similar conditions (Supporting Information), and they parallel those reported for other Rh_2^{5+} bimetallic cores.[72]

Additional evidence for a new electronic transition arising from coordination of the halide ion following the photochemical reaction is shown in Figure 5b, where the absorption spectra of photochemically generated $[Rh_2(m\text{-}OCH_3\text{-form})_4]Br$ ($\lambda_{irr} \geq$ 435 nm, 5 min, 30 mM CBr_4 in acetone) is compared to that of the complex oxidized with excess $AgBF_4$ in acetone in the presence of $(t\text{-Bu})_4NBr$. In both spectra (Figure 5b), the peak at ∼670 nm arises from the coordination of the bromide ion to the axial position of the oxidized dirhodium core. This peak is not observed if the chemical oxidation is conducted in the absence of a bromide source in acetone. The identity of this peak will be discussed below.

The oxidative addition of alkyl halides to metal complexes has been shown to result in the formation of axially coordinated metal halide complexes,[72−74] alkyl metal complexes,[75] or alkyl halide metal complexes.[76−78] The latter two can be ruled out in this case because the axial position of these complexes is too sterically crowded by the formamidinate ligands to support coordination of the alkyl group. Axially coordinated structures of $Rh_2(form)_4$ solved to date show the presence of only linear ligands, such as CO and CN^-.[65,66] This observation is markedly different from the axial coordination of sterically demanding ligands to other dirhodium paddle wheel complexes with more accessible axial sites.[79,80] Therefore, it is unlikely that the photochemical reactions of the dirhodium formamidinates and $Rh_2(tpgu)_4$ with alkyl halides result in the axial coordination of the alkyl fragments to the dirhodium core.

The MALDI-TOF mass spectrum of $Rh_2(tpgu)_4$ photolyzed in $CHBr_3$ exhibits a parent ion peak consistent with the $Rh_2(tpgu)_4Br$ species at m/z = 1430.5. The formation of the mixed-valent dirhodium cation with the axially coordinated halide is evident in the X-ray crystal structure of $Rh_2(p\text{-MeO-form})_4Cl$ (Figure 6). The $Rh_2(p\text{-MeO-form})_4Cl$ crystals were

(72) Cotton, F. A.; Daniels, L. M.; Murillo, C. A.; Timmons, D. J.; Wilkinson, C. C. *J. Am. Chem. Soc.* **2002**, *124*, 9249.
(73) Hsu, T.-L. C.; Chang, I.-J.; Ward, D. L.; Nocera, D. G. *Inorg. Chem.* **1994**, *33*, 2932.
(74) Hsu, T.-L. C.; Engebretson, D. S.; Helvoit, S. A.; Nocera, D. G. *Inorg. Chim. Acta* **1995**, *240*, 551.
(75) Cooksey, C. J.; Dodd, D.; Gatford, C.; Johnson, M. D.; Lewis, G. J.; Ttchmarsh, D. M. *J. Chem. Soc., Perkin Trans.* **1972**, *2*, 655.
(76) Fitton, P.; Johnson, M. P.; McKeon, J. E. *Chem. Commun.* **1968**, 6.
(77) Klabunde, K. J. *Acc. Chem. Res.* **1975**, *8*, 393.
(78) Von Zelewsky, A.; Suckling, A. P.; Stoecki-Evans, H. *Inorg. Chem.* **1993**, *32*, 4585.
(79) Christoph, G. G.; Halpern, J.; Khare, G. P.; Koh, Y. B.; Romanowski, C. *Inorg. Chem.* **1981**, *20*, 3029.
(80) Cotton, F. A.; Felthouse, T. R.; Klein, S. *Inorg. Chem.* **1981**, *20*, 3037.

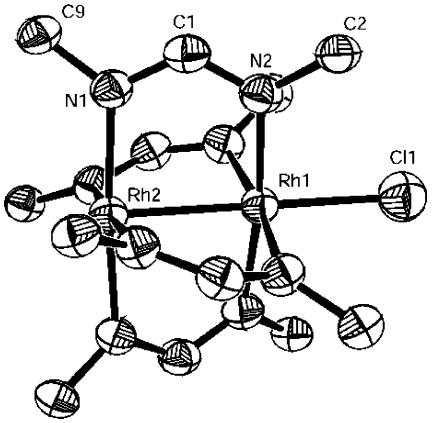

Figure 6. ORTEP representation of Rh_2(*p*-MeO-form)$_4$Cl with thermal ellipsoids drawn at the 50% probability level. Only the core atoms of the complex and the ipso carbons of the phenyl rings are shown for clarity.

collected from the reaction of Rh_2(*p*-MeO-form)$_4$ in $CHCl_3$ exposed to room light for 24 h, followed by slow solvent evaporation. They exhibit Rh−Rh, Rh−N, and Rh−Cl bond lengths of 2.4670(7), 2.046(2), and 2.400(2) Å, respectively (Table 2). These distances are similar to those of other Rh_2^{5+} complexes with nitrogen equatorial bridging ligands and an axial chloride, some of which are listed in Table 2.[81]

The products that result from the photolysis of Rh_2(tpgu)$_4$ in brominated solvents possess an absorption band at ~800 nm. This peak is blue-shifted in the photolysis experiments conducted with the corresponding bimetallic complex in chlorinated solvents, and typically appears as a shoulder at ~650 nm. The shift of this peak is consistent with a ligand-to-metal charge transfer (LMCT) transition from the halide to the oxidized dirhodium core. The 2884 cm^{-1} shift is expected because of the difference in the oxidation potential of the halides, and it is typical for LMCT transitions involving M−Cl and M−Br, such as in $Rh(NH_3)_5X$ ($X^- = Cl^-, Br^-$).[82,83] Similar results were observed for the Rh_2(R-form)$_4$ complexes.

Reaction Mechanism. Halogen atom abstraction from alkyl halides by the Rh_2^{4+} complexes upon irradiation to form the corresponding Rh_2^{5+}−X (X = Cl, Br) may involve the formation of alkyl radicals as shown in eq 1.

$$Rh_2(L)_4 + RX \xrightarrow{h\nu} Rh_2(L)_4{-}X + R^{\bullet} \qquad (1)$$

In solution, the reaction of two alkyl radicals would result in the production of the corresponding R_2 dimerization product in the absence of other species with which R• can react efficiently. Indeed, the photochemistry of Rh_2(*p*-CF_3-form)$_4$ ($\lambda_{irr} \geq 435$ nm) with benzyl bromide followed by ^{1}H NMR in acetone-d_6 results in the disappearance of the signal at 4.64 ppm assigned to the methylene protons of the starting material, $BrCH_2(C_6H_5)$, and the concomitant appearance of the corresponding signal for dibenzyl at 3.30 ppm. These results point at the formation of R• as described by eq 1 and are typical of the photochemical generation of alkyl radicals.[84]

The reaction in eq 1 can proceed via outer-sphere or inner-sphere mechanisms, given by eq 2 and 3, respectively.[85]

$$*Rh_2(L)_4 + RX \xrightarrow{ET} [Rh_2(L)_4]^+ + RX^- \xrightarrow{fast} Rh_2(L)_4X + R^{\bullet} \qquad (2)$$

$$*Rh_2(L)_4\cdots XR \rightarrow Rh_2(L)_4X + R^{\bullet} \qquad (3)$$

In the outer-sphere case (eq 2), the initial excited state electron transfer from $*Rh_2(L)_4$ generates RX^-, a species that is well-known to undergo fast dissociation to produce halide and alkyl radicals.[86,87] Therefore, the rate of the outer-sphere reaction is expected to depend on the reduction potential of RX.[88] Alternatively, the rate of an inner-sphere reaction should be sensitive to the carbon-halogen bond dissociation energy of the alkyl halide, steric effects of the alkyl group, and the nature of the halogen.[89−91]

Semilog plots of the relative rate of product formation versus the carbon-halogen bond dissociation energy, E(C−X),[85,92] and versus the irreversible reduction potential of the alkyl halides, E_p,[85] are shown in Figure 7 for the photolysis of Rh_2(tpgu)$_4$. It is evident from the two plots in Figure 7 that a better correlation of the relative rates of these reactions is obtained with E_p than with E(C−X), indicative of an outer-sphere pathway (eq 2). The same trend was observed for the photochemistry of Rh_2(*p*-CF_3-form)$_4$ and Rh_2(*p*-MeO-form)$_4$ with various alkyl chlorides and alkyl bromides. The lack of photoreactivity of Rh_2(tpgu)$_4$ toward CH_3I and C_2H_5I provides further evidence of an outer-sphere mechanism (eq 2). The C−I bond dissociation energies of CH_3I and C_2H_5I are 236 and 259 kJ/mol,[85] respectively, corresponding to weaker bonds than those of CH_2Br_2, $CHBr_3$, and CCl_4, all of which react with the dirhodium complexes upon irradiation with visible light (Figure 7b). However, both CH_3I and C_2H_5I are harder to reduce than the alkyl halides that react with Rh_2(R-form)$_4$ (R = *p*-CF_3, *p*-Cl, *p*-OCH_3, *m*-OCH_3) and Rh_2-(tpgu)$_4$ (Figure 7a) with $E_p = -1.41$ V and -1.45 V vs NHE.[85]

Although the photolysis of Rh_2(R-form)$_4$ (R = *p*-CF_3, *p*-Cl, *p*-OCH_3, *m*-OCH_3) and Rh_2(tpgu)$_4$ in CCl_4 result in similar spectral changes, their reaction rates differ significantly. The relative production of the corresponding oxidized product following irradiation of each complex with $\lambda_{irr} \geq 435$ nm

(81) Yang, Z.; Ebihara, M.; Kawamura, T.; Okubo, T.; Mitani, T. *Inorg. Chim. Acta* **2001**, *321*, 97.
(82) Endicott, J. F. In *Concepts of Inorganic Photochemistry*; Adamson, A. W., Fleischauer, P. D., Eds.; Wiley-Interscience: New York, 1975; pp 84−85.
(83) Jørgensen, C. K. *Absorption Spectra and Chemical Bonding in Complexes*; Pergamon Press: London, 1962.
(84) Noh, T.; Lei, X.-G.; Turro, N. J. *J. Am. Chem. Soc.* **1993**, *115*, 3105.
(85) Howes, K. R.; Bakac, A.; Espenson, J. H. *Inorg. Chem.* **1988**, *27*, 3147.
(86) Andrieux, C. P.; Merz, A.; Saveant, J.-M. *J. Am. Chem. Soc.* **1985**, *107*, 6097.
(87) Andrieux, C. P.; Gallardo, I.; Saveant, J.-M.; Su, K.-B. *J. Am. Chem. Soc.* **1986,** *108*, 638.
(88) Marzilli, L. G.; Marzilli, P. A.; Halpern, J. *J. Am. Chem. Soc.* **1970**, *92*, 5752.
(89) Halpern, J.; Maher, J. P. *J. Am. Chem. Soc.* **1964**, *86*, 2311.
(90) Halpern, J.; Maher, J. P. *J. Am. Chem. Soc.* **1965**, *87*, 5361.
(91) Chock, P. B.; Halpern, J. *J. Am. Chem. Soc.* **1969**, *91*, 582.
(92) Lide, D. R. *CRC Handbook of Chemistry and Physics*, 71st ed.; CRC Press: Boston, MA, 1990.

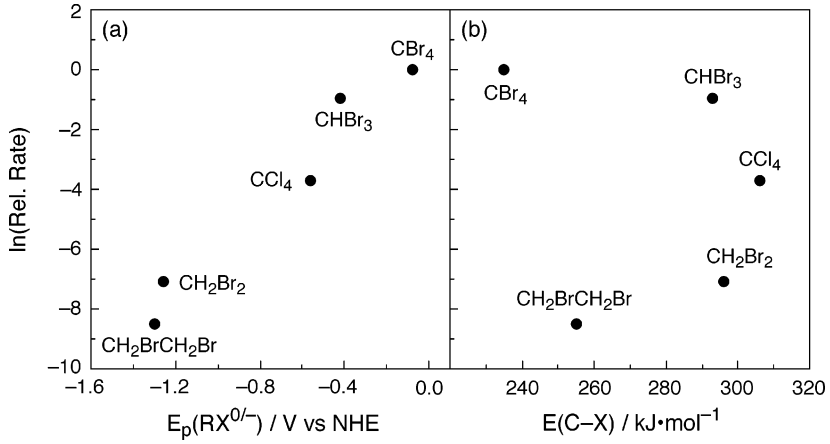

Figure 7. Semilog plots of the relative rate of the photochemistry of $Rh_2(tpgu)_4$ ($\lambda_{irr} \geq 435$ nm) as a function of (a) irreversible reduction potential (from ref 85) and (b) C−X (X = Cl, Br) bond dissociation energy of the alkyl halides (from refs 85, 92). The depletion of the reactant concentration as a function of time was monitored using its absorption at 881 nm.

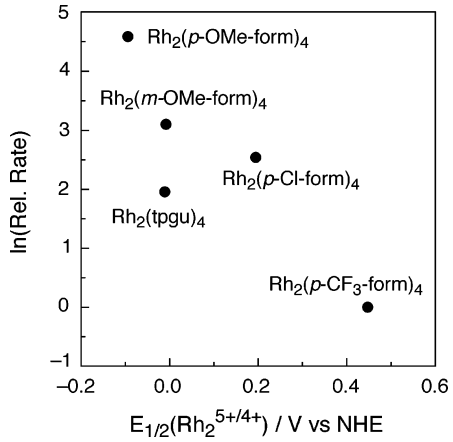

Figure 8. Semilog plots of the relative rate of the photochemistry of the dirhodium complexes, $Rh_2(L)_4$ ($\lambda_{irr} \geq 435$), as a function of $E_{1/2}(Rh_2^{5+/4+})$. The formation of the product was monitored as a function of time using its absorption at ~1000 nm.

for 20 min is shown in Figure 8, plotted as a function of the complex oxidation potential. The semilog plot of the relative reaction rate vs $E_{1/2}(Rh_2^{5+/4+})$ shown in Figure 8 exhibits a nearly linear relationship for the dirhodium tetraformamidinates, $Rh_2(R\text{-form})_4$ (R = *p*-CF_3, *p*-Cl, *p*-OCH_3, *m*-OCH_3), as expected for an outer-sphere mechanism. The slight deviation of $Rh_2(tpgu)_4$ from the linear relationship in the plot shown in Figure 8 may be the result of the larger average radius of this complex relative to the formamidinates, which would increase the distance between the bulk alkyl halide and the redox-active Rh_2^{4+} core. Such an increase in distance is known to have a profound effect on bimolecular electron transfer rates through a reduction in electronic coupling, which depends exponentially on donor-acceptor separation.[93] A similar trend is observed when the reaction quantum yields of the complexes in CCl_4 are plotted vs $E_{1/2}(Rh_2^{5+/4+})$ values listed in Table 3.

(93) Turro, C.; Zaleski, J. M.; Karabatsos, Y. M.; Nocera, D. G. *J. Am. Chem. Soc.* **1996**, *118*, 6060.

Conclusions

The substituted dirhodium(II,II) tetraformamidinates, $Rh_2(R\text{-form})_4$ (R = *p*-CF_3, *p*-Cl, *p*-OCH_3, *m*-OCH_3), and the new complex $Rh_2(tpgu)_4$ are able to undergo one electron oxidation and reduce alkyl halides upon irradiation with visible light. The synthesis and characterization of the complexes is reported, and the crystal structure of $Rh_2(tpgu)_4$ is presented. The complexes react with chlorinated and brominated molecules under low energy irradiation ($\lambda_{irr} \geq 795$ nm) but not when kept in the dark. The metal-containing product of the photochemical reaction with RX (X = Cl, Br) is the corresponding oxidized Rh_2^{5+}−X (X = Cl, Br) complex, and the crystal structure of photochemically generated $Rh_2(p\text{-}OCH_3\text{-form})_4Cl$ is presented. In addition, the product resulting from the dimerization of the alkyl fragment, R_2, is also formed. A comparison of the dependence of the relative reaction rates on the reduction potentials of the alkyl halides and their C−X bond dissociation energies are consistent with an outer-sphere mechanism. In addition, the relative reaction rates of the metal complexes with CCl_4 decrease with the oxidation potential of the dirhodium complexes. If the reduced dirhodium complexes can be regenerated to complete the catalytic cycle, the ability of these compounds to utilize lower energies than those previously reported would make these promising systems for photoremediation reactions with alkyl halides.

Acknowledgment. C.T. thanks the National Institute of Health (RO1 GM64040-01) for their generous support. The authors thank Jason D'Acchioli for assistance with calculations conducted at the Ohio State Supercomputer Center.

Supporting Information Available: Crystallographic data in CIF format and the EPR spectrum of $[Rh_2(p\text{-}CF_3\text{-form})_4]^+$. This material is available free of charge via the Internet at http://pubs.acs.org.

IC048377J